ACS Catalysis

pubs.acs.org/acscatalysis

Research Article

# One-Pot Conversion of Acetone into Mesitylene over Combinations of Acid and Basic Catalysts

Laura Faba, Juan Gancedo, Jorge Quesada, Eva Diaz, and Salvador Ordóñez*

Cite This: *ACS Catal.* 2021, 11, 11650–11662

Read Online

ACCESS | Metrics & More | Article Recommendations | Supporting Information

**ABSTRACT:** The transformation of acetone (a byproduct of phenol manufacturing or a bioderived chemical) into mesitylene is a very attractive reaction to prepare renewable fuels and chemicals. This reaction has been studied over both base and acid catalysts, with relevant limitations (side reactions over acid catalysts, oligomerization of isophorones over basic materials, etc.). We propose an alternative strategy to perform this reaction combining acid and basic catalysts either as separate beds or as mechanical mixtures. For this purpose, we first study the reaction over five representative materials ($\beta$-zeolite, Al-MCM-41, Mg−Al mixed oxide, MgO, and $TiO_2$). These studies allow determining the rate-limiting steps and identifying the most relevant catalytic properties to enhance the selectivity toward mesitylene, minimizing the deactivation produced by the permanent adsorption and oligomerization as well as side reactions yielding undesired products ($\beta$-scissions). Once the combining strategies are studied, we propose using double beds of Al-MCM-41 and $TiO_2$ as the optimum approach. The observed synergistic effects enhance the mesitylene productivity by more than 57% to the most active catalyst (Al-MCM-41), working at a low temperature (250 °C). This improvement is due to the activity of the base catalyst ($TiO_2$), producing an optimum mixture of mesityl oxide and acetone that contacts with the acid catalyst (Al-MCM-41), where the second condensation and dehydration steps are so fast that the mesitylene production is stable, not being affected by any deactivation process.

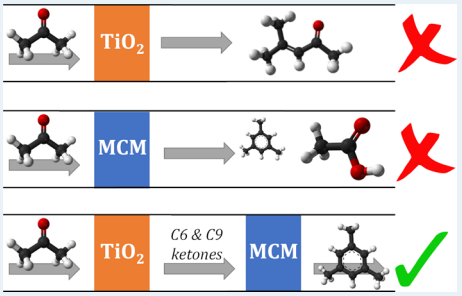


**KEYWORDS:** *aldol condensation, aluminosilicates, cyclization, dehydration, mechanical mixture, trimethylbenzenes*



## INTRODUCTION

Mesitylene (1,3,5-trimethylbenzene) is a high-value chemical, being an intermediate for different manufacturing processes because of its high reactivity (it can be alkylated, nitrated, sulfated, or halogenated).[1−3] Its main applications are in organic synthesis (e.g., antioxidants and thermal stabilizers for polymers, plant growth regulators, dye intermediates, contaminant scavenging agents, explosives, and so forth) and the production of high-octane additives to liquid fuels.[4−6]

Traditional routes to produce it, as pseudocumene isomerization, use petroleum as a raw material,[7] owning a nonrenewable character. Furthermore, these routes have technical drawbacks due to the difficulties isolating products with similar boiling points (e.g., mesitylene and 2-ethyltoluene, 165 °C). In this context, the development of alternative routes using renewable raw materials and solid catalysts is one of the main challenges of chemical engineering, with the acetone route being one of the most promising ones.[8,9]

The production of mesitylene using acetone as a building block is a complex reaction, combining the self-condensation of acetone molecules with cross condensation between acetone and other acetone condensation adducts, following the pathways depicted in Scheme 1.[10] The boiling points of the products involved in this reaction are significantly different from that corresponding to mesitylene (56 °C of acetone, 129.5 °C of mesityl oxide, 198 °C of phorones, and 215.2 °C of isophorones), minimizing purification problems. It is well known that both bases and acids can be used as catalysts, obtaining the same products by different mechanisms.[11] Thus, basic materials abstract a proton for the $\alpha$-carbon and form an enolate that attacks a nearby electrophile to form the C−C bond, that is, the diacetone alcohol. The same compound is obtained when using acids but after the protonation of the oxygen of the carbonyl group that, by resonance equilibrium, produces the abstraction of the most positively charged proton, the one from the $\alpha$-carbon. This abstraction is required to promote the bimolecular C−C coupling step.

In presence of weak acidity or acid−basic pairs, the diacetone alcohol undergoes dehydration reactions, yielding mesityl and isomesityl oxide, the main C6 compounds. If the reaction is carried out in the gas phase (i.e., high temperatures) and the active sites are strong enough, the mesityl oxide undergoes a subsequent condensation with a second acetone

Received: July 9, 2021
Published: September 4, 2021





https://doi.org/10.1021/acscatal.1c03095
*ACS Catal.* 2021, 11, 11650–11662

**Scheme 1. Reaction Pathways for Acetone Upgrading to Mesitylene (Solid Arrows) and C=C $\beta$-Scission Side Reaction (Dashed Arrow); Codes: (A) Mesityl Oxide, (B) Isomesityl Oxide, (C) Phorones, (D) $\alpha$-Isophorone, (E) $\beta$-Isophorone, (F) Isobutene, and (G) Acetic Acid**

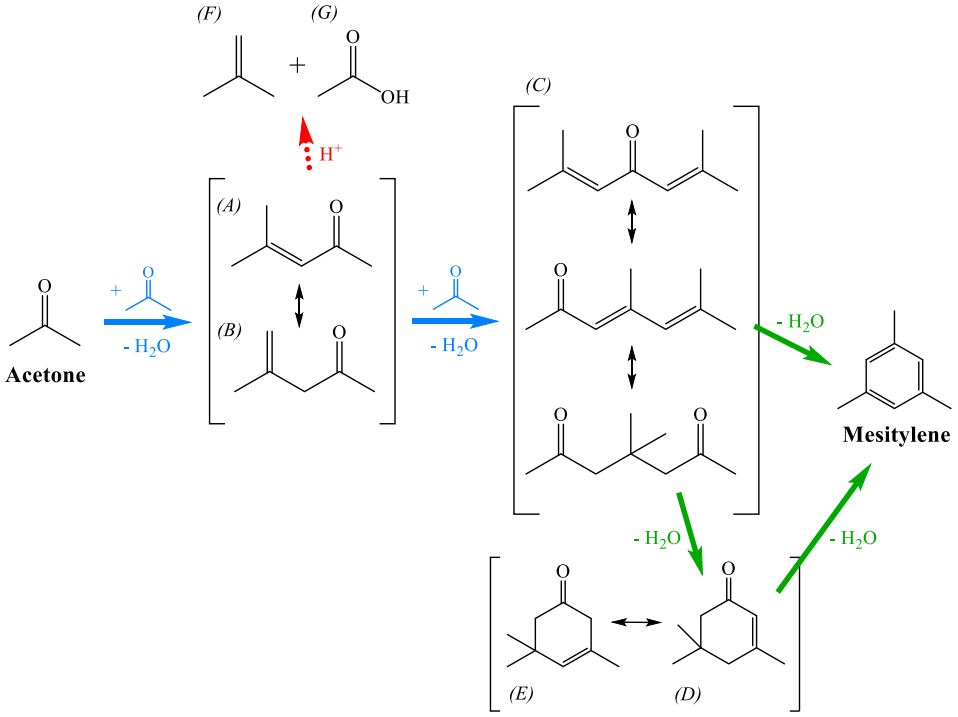


molecule, yielding linear ketones called phorones (three isomers identified). Different reactions produce $\alpha$- and $\beta$-isophorones and mesitylene (the target compound). According to the literature, the mesitylene formation can involve the dehydration−cyclization of phorones catalyzed by acid−base pair sites through a proton abstraction or the dehydration by the $E_2$ mechanism of isophorones, involving acid sites.[12]

Several basic catalysts have been proposed for the gas-phase acetone valorization: $TiO_2$, $ZrO_2$, Mg−Zr, and Mg−Al mixed oxides among others.[12−15] Nevertheless, these studies were proposed to optimize the isophorone production, being in all the cases characterized by a low selectivity to mesitylene (because of their low acidity). In addition, the strong basicity is related to coke production by phorone and isophorone oligomerization.[16] On the other hand, acid materials such as microporous and mesoporous aluminosilicates have been also proposed, catalyzing the acetone condensation by Brønsted or Lewis acidic sites (i.e., protons or metal cations, respectively) and promoting the mesitylene production ($E_2$ mechanism).[17−19] However, this acidity also promotes the mesityl oxide cracking by $\beta$-scission, indicated with a dashed line in the scheme, a non-desired reaction that produces isobutene and acetic acid and, to a lesser extent, other light alkenes.[20] This reaction strongly limits their application since acetates and their oligomers are involved in the catalytic deactivation by solid deposition.[10,20]

In conclusion, the mesitylene formation by acetone condensation is not optimized, and the previous literature suggests that an appropriate balance between acid and basic sites is needed. However, too strong basicity or acidity enhances the formation of undesired byproducts, such as alkenes or heavy oligomers. This optimization requires a clear identification of the involved catalytic sites to distinguish if there is a preferential phorone that produces mesitylene (and which sites promote its formation) or if the acid sites required to promote the $E_2$ mechanism must be isolated or close to other types of sites that stabilize any reaction intermediate.

This study proposes a new approach based on a double-catalytic system, combining a basic metal oxide (anatase $TiO_2$, MgO, Mg−Al mixed oxide) and acidic aluminosilicates (microporous $\beta$-zeolite or mesoporous Al-MCM-41) with different configurations (independent successive beds and the mechanical mixture). It is expected that the base catalyst promotes the first steps of the process, whereas the acid catalyst improves the dehydration−cyclization steps. The relevance of the $\beta$-scission is supposed to be lower after preventing the stable adsorption of mesityl oxide that favors it. The different basicity and acidity of these materials could give relevant information about the preferential mechanisms by individual studies, whereas the comparison between single beds, double beds, and mechanical mixtures could complete this study identifying the vicinity requirements. As consequence, a relevant improvement in the mesitylene production as well as in the catalytic stability is expected by the synergetic effect of both catalytic activities.

## MATERIALS AND METHODS

**Materials.** Three commercial materials are used as catalysts: anatase $TiO_2$ (99.8%, Aldrich), $NH_4^+$−$\beta$-zeolite (Si/Al = 12.5, Zeolyst, CP814E), and $H^+$-Al-MCM-41 (Si/Al = 39.5, Aldrich, 643653). Prior to performing catalytic activity experiments, $TiO_2$ powder was pretreated in air by heating up from 20 to 450 °C at 10 °C·min$^{-1}$, keeping the final temperature for 3 h. $NH_4^+$−$\beta$-zeolite was thermally treated to desorb binding $NH_3$ with the aim of bringing its active form (i.e., protonated state: $H^+$-$\beta$-zeolite). Thus, it was pretreated in air from 20 to 550 °C at 1 °C·min$^{-1}$ of heating rate, keeping the final temperature for 12 h. This thermal treatment was also


https://doi.org/10.1021/acscatal.1c03095
ACS Catal. 2021, 11, 11650−11662

carried out in the case of $H^+$-Al-MCM-41 to follow the same sample preparation procedure with both aluminosilicates, although it was initially in its protonated form. In addition, two oxides were prepared in the lab, MgO and Mg−Al mixed oxide, following the procedures previously reported in the literature.[13,21] All the catalysts were then pelletized separately by pressing at 92.5 MPa, crushed, and sieved to obtain 250−355 $\mu$m aggregates. Mixtures of powders with a mass relation of 1:1 were also pelletized following the same procedure, resulting in mechanical mixture catalysts. Al-MCM-41 and the Mg−Al mixed oxide will be defined from now as Al-MCM and MgAl, respectively.

**Catalyst Characterization.** The active site distributions and strengths were determined by temperature-programmed desorption (TPD) of probe molecules, $NH_3$ and $CO_2$, for the acidity and basicity, respectively. Samples of 60 mg were pretreated in helium flow at 300 °C during 0.5 h to ensure a clean surface. Subsequently, the catalyst was cooled down to 30 °C and saturated in a flow of the probe molecule (10% in the case of $CO_2$, 2.5% for $NH_3$) for 1 h. After stabilization, the concentration of active sites was quantified by monitoring the evolution of the desorbed species ($NH_3$ and $CO_2$) by mass spectroscopy as a function of the temperature, heating up the system from 30 to 950 °C with a 5 °C·min$^{-1}$ rate. The TPD-mass spectrometry (MS) unit was composed of a Micromeritics AutoChem II 2920 coupled to a Pfeiffer Vacuum Omnistar Prisma mass spectrometer.

The textural analyses were done by $N_2$ physisorption in a Micromeritics ASAP 2020, applying the *t*-plot method to determine the micropore volume and external area; the Barrett−Joyner−Halenda method to quantify the mesopore volume and pore area; and the Brunauer−Emmett−Teller method to measure the total surface area.

Coke deposited on the catalytic surfaces was analyzed by temperature-programmed oxidation (TPO) analyses in a Micromeritics Autochem II 2920. Initially, a flow of helium (20 mL/min) was used to clean the surface of the spent catalyst recovered after the reaction. The temperature was kept at 150 °C for 30 min using a 5 °C/min slope to reach the set point. Coke combustion was carried out with a flow of 5% $O_2$ in helium (20 mL/min STP), increasing the temperature up to 950 °C, with a 2.5 °C/min rate. The $CO_2$ effluent was analyzed by MS (Omnistar GSD 301).

**Catalytic Activity Studies.** Reactions were performed in a U-shaped fixed-bed reactor made of quartz (8.0 mm i.d.) using 200 mg of the catalyst or the mechanical mixture, as appropriate. The double-bed configuration involves first the basic catalyst and then the acidic one, with both beds being separated by a quartz plug. This configuration is studied employing 100 and 200 mg of each catalyst. The temperature was kept at the set point (from 200 to 400 °C, as a function of the experiment) using a PID-controlled furnace and a K-type thermocouple located close to the upper surface of the catalytic bed. Experiments were carried out with an inlet pressure of 250 kPa, observing a pressure drop lower than 10 kPa in all cases.

Acetone (≥99.9%, VWR) is injected using a liquid syringe pump into a helium stream with a flow rate of 1 cm$^3$·h$^{-1}$, being suddenly vaporized in the transfer line, heated at 250 °C. It results in a reactor inlet stream with an acetone concentration of 20 vol % (50 kPa of partial pressure).

The reactor outlet-gas mixture was analyzed on-line using an HP 6890Plus gas chromatograph equipped with a flame ionization detector (GC-FID) and a TRB-5MS capillary column (30 m, 0.25 mm, 0.25 $\mu$m) as the stationary phase. Both retention times and response factors of acetone and the main reaction products were determined by calibrations with commercial standards. The complete identification of all the peaks was obtained by GC−MS (GC−MS Shimadzu QP 2010) after condensing the effluent in an ice bath using both the same column and temperature method as in the GC-FID. In the case of isobutene and mesitylene isomers (other alkylbenzenes), the calibration line of each compound was calculated from that of its most similar species (reference, e.g., mesityl oxide, phorones, mesitylene) by using a response factor.[22] Henceforth, during reaction tests, the percentages of known compound areas were higher than 98%.

Quantitative analysis was done considering the parameters explained in eqs 1−3. Thus, conversions were calculated by the difference between inlet and outlet acetone concentrations. The carbon balance closure was used to determine the accuracy of these discussions, and the discrepancies in the carbon balances were assumed to be due to the formation of coke, char, condensed compounds, and CO and/or $CO_2$, naming this group as "COx & coke". Product selectivities were calculated in the mole of carbon basis excluding the reactant and yields resulting from the multiplication of the conversion and selectivity. In the equations, "C" is the concentration and "*n*" is the number of carbon atoms of "a" (acetone) or every "*i*" product.

$$\text{Conversion, } x\ (\%) = \left(1 - \frac{C_{a,\text{outlet}}}{C_{a,\text{inlet}}}\right)\cdot 100 \tag{1}$$

$$\text{carbon balance closure: CB}\ (\%) = \frac{\sum (n_i \cdot C_i) + n_a \cdot C_{as}}{n_a \cdot C_{a0}}\cdot 100 \tag{2}$$

$$\text{selectivity}\ (\%) = \frac{n_i \cdot C_i}{\sum (n_i \cdot C_i)}\cdot \text{CB}\cdot 100 \tag{3}$$

## RESULTS AND DISCUSSION

**Single Catalyst Performance: Comparison of Acid and Basic Routes.** The acid and base catalysts were tested separately to identify the best conditions enabling the highest activity and selectivity to the target compound (mesitylene), minimizing the role of the $\beta$-scission and possible oligomerization side reactions. The experiments were carried out in the range of temperatures from 200 to 400 °C, feeding 1 cm$^3$·h$^{-1}$ of a 20% acetone in helium stream (WHSV = 4 h$^{-1}$), analyzing the conversion, the concentration, and the yield evolution for 6 h of time on stream (TOS).

External and internal diffusional limitations were evaluated based on experimental data obtained with each material using Mear's criterion ($C_M$) for the external diffusion and the Thiele modulus ($\phi$) and the effectiveness factor ($\eta$) through the Weisz−Prater parameter ($C_{WP}$) for the internal one. The procedure followed has been detailed in our previous work, explaining all the correlations and coefficients used, together with the physical and chemical properties, to assess these parameters.[17] The results are summarized in the Supporting Information, Table S1. According to these values, the external resistance diffusion is negligible since all the materials fulfil Mears's criterion, obtaining values up to 6 orders of magnitude lower than the threshold (0.15). $C_{WP}$ values are lower than unity except in the case of $\beta$-zeolite (1.19). Even in this case,


https://doi.org/10.1021/acscatal.1c03095
ACS Catal. 2021, 11, 11650−11662

total control of internal diffusion ($C_{WP} \gg 1$) is discarded, but its relevance cannot be neglected. The lowest mass-transfer effects of the internal diffusion limitation are observed for $TiO_2$ with an effectiveness factor close to 90%, whereas this value decreases up to 2.4% in the case of $\beta$-zeolite, in agreement with the higher internal diffusion limitations. This behavior is due to the similar size between the reactant molecule and $\beta$-zeolite's voids and must be considered to explain its catalytic behavior.

Figure 1 shows the evolution of the acetone initial conversion ($x_0$) as a function of the temperature, observing a large difference in behavior between both kinds of catalysts. Thus, the highest conversions are reached with the acid materials, with values from 67.2 to 98.1% with $\beta$-zeolite and from 55.0 to 80.8% with Al-MCM. Similar conversions are obtained with the three basic materials tested, achieving values significantly lower than those reached with the acid ones (from 15.4 to 45.6% with MgAl and from 14 to 42% with MgO). As for $TiO_2$, a material in which basicity coexists with redox activity, it shows a parallel evolution to the basic materials at the lowest temperatures (12.4% at 200 °C) and a softer increase with the temperature, reaching only 26.9% of conversion at 400 °C. To sum up, despite the similar values obtained at low temperatures, conversions observed at higher temperatures increase as the medium-strength basicity and the medium-strength base−acid pairs of these materials increase (characterization results summarized in Table 1), discarding any influence of redox properties of $TiO_2$ on this parameter. This fact suggests that the acetone conversion is mainly determined by the first condensation and dehydration step (mesityl oxide formation), whereas the second condensation and the subsequent dehydration and cyclization steps (acid catalysis involved) do not have enough strength to shift the reaction toward higher conversions. However, there is not a constant ratio between conversion and basicity; that is, different TOF values (calculated as the normalized conversion: $x_0$/[medium-strength basicity]) are reached with each material, with values from 0.95 of $TiO_2$ to 0.64 of MgAl, suggesting different catalytic capacities of these sites depending on the catalyst.

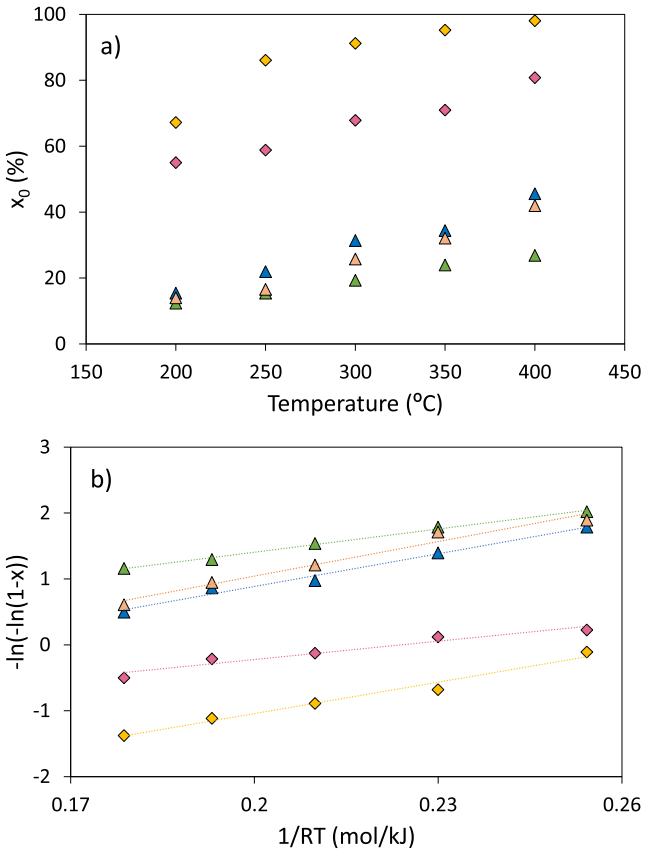


**Figure 1.** (a) Evolution of the initial conversion with the temperature and (b) Arrhenius plot for acetone conversion considering pseudo-first-order kinetics for the acetone conversion rate. Symbols: (orange ◆) $\beta$-zeolite, (pink ◆) Al-MCM, (green ▲) $TiO_2$, (blue ▲) MgAl, and (peach ▲) MgO.

**Table 1. Morphological and Physicochemical Properties of Catalysts Used in This Work after the Pretreatment**

| | catalyst | | | | |
|---|---|---|---|---|---|
| | $TiO_2$ | MgO | MgAl | $\beta$-zeolite | Al-MCM |
| Si/Al | | | | 12.5 | 39.5 |
| surface area ($m^2 \cdot g^{-1}$) | 12 | 43 | 109 | 620 | 966 |
| pore diameter (Å) | 218 | 141 | 83 | 10 | 42 |
| basicity (mmol $CO_2 \cdot g^{-1}$) | 0.24 | 0.42 | 0.81 | 0.05 | 0.10 |
| weak (<250 °C) | 0.08 | 0.11 | 0.34 | 0.01 | 0.05 |
| medium (250−450 °C) | 0.13 | 0.24 | 0.25 | 0.02 | 0.02 |
| strong (>450 °C) | 0.03 | 0.07 | 0.22 | 0.02 | 0.03 |
| acidity (mmol $NH_3 \cdot g^{-1}$) | 0.03 | 0.15 | 0.32 | 10.13 | 1.09 |
| weak (<250 °C) | 0.02 | 0.07 | 0.10 | 5.08 | 0.36 |
| medium (250−450 °C) | 0.01 | 0.01 | 0.09 | 4.33 | 0.30 |
| strong (>450 °C) | | 0.06 | 0.13 | 0.72 | 0.43 |

Parallel analysis with the acid materials is not possible since the mass-transfer limitation controls the activity of $\beta$-zeolite, preventing the comparison with the Al-MCM results. In general, these catalysts appear to be more active than the basic ones. However, the different concentration of active sites (the concentration of acid sites in acid materials is 1 order of magnitude higher than that of the basic ones in base catalysts) could alter the correct analysis of these data, therefore requiring a normalized value.

With this aim, initial conversions were used to estimate the initial reaction rates ($r_0$) considering the space velocity (SV), according to the discussion detailed in our previous work,[17] and these rates were normalized by the total amount of acid or basic sites (as a function of the catalyst) to complete the discussion, obtaining the following equation (eq 4):

$$r_0 = \frac{x_0 \cdot SV}{[\text{acidity}]\text{or}[\text{basicity}]} \quad (4)$$

These results are detailed in Table 2. The values obtained indicate that despite the temperature analyzed, $TiO_2$ catalytic sites are the most active ones. Thus, at 400 °C, $r_0$ reaches values of 1.1 and 1.5 times higher than the corresponding ones for MgO and Al-MCM, respectively. The low value reached with $\beta$-zeolite is justified by the microporous character of this catalyst, leading to the presence of non-accessible active sites within its framework. $\beta$-zeolite and Al-MCM contain acid sites of similar strength (Table 1), but they are placed inside pores of very different sizes and connectivities, creating diverse reactivities.[23]

This behavior is not evident in basic materials since all of them are mesoporous ones. In this case, the different values support the hypothesis that the total concentration of basic sites is not so important, with the strength distribution of these


https://doi.org/10.1021/acscatal.1c03095
ACS Catal. 2021, 11, 11650−11662

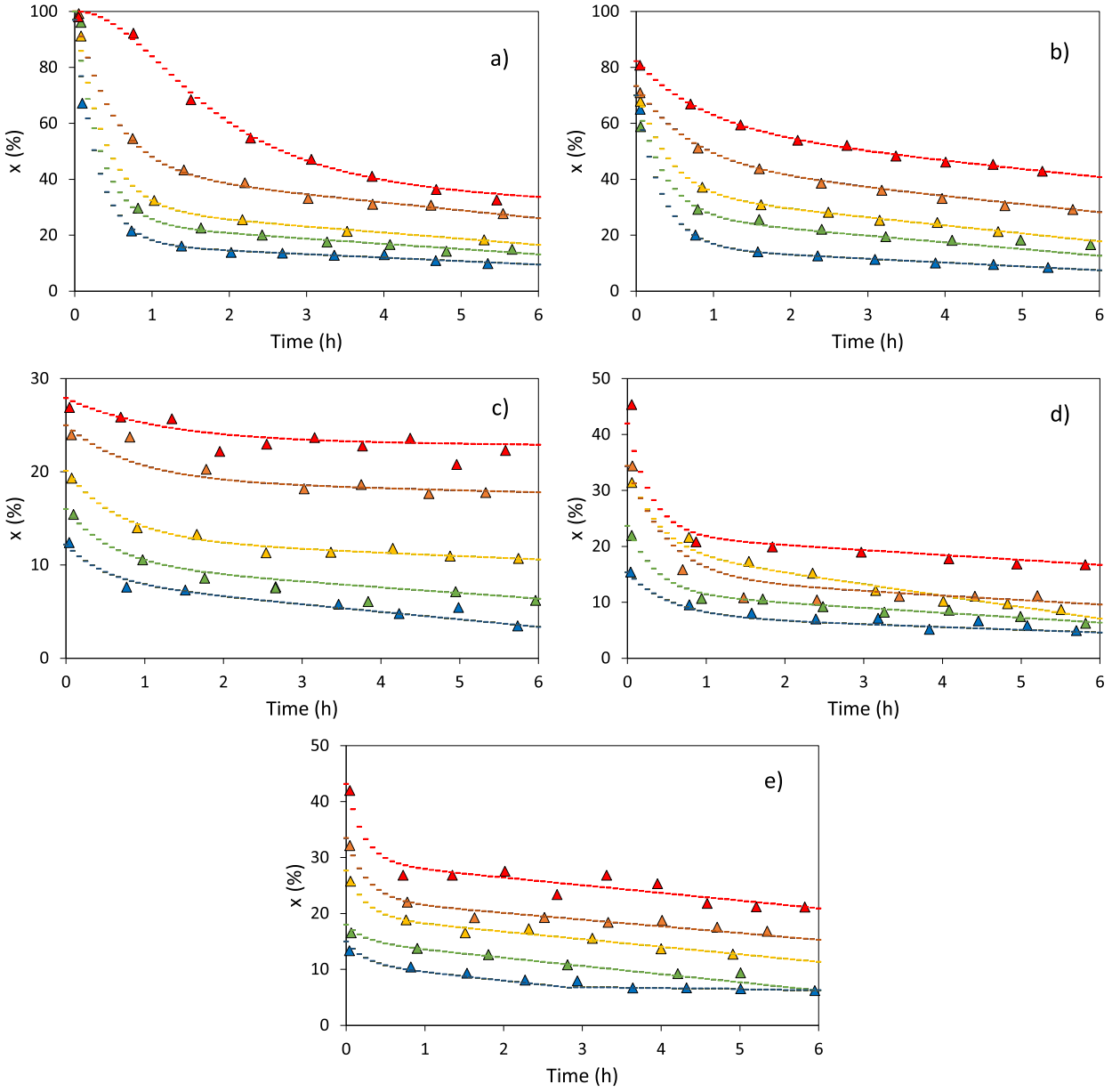


**Figure 2.** Evolution of acetone conversion with TOS as a function of the reaction temperature. The results correspond to (a) $\beta$-zeolite, (b) Al-MCM, (c) $TiO_2$, (d) MgAl, and (e) MgO. Symbols correspond to experimental points, and dashed lines correspond to the deactivation kinetic adjustment. Symbols: (blue ▲) 200 °C, (green ▲) 250 °C, (orange ▲) 300 °C, (brown ▲) 350 °C, and (red ▲) 400 °C.

sites being more relevant. On the other hand, the specificity of one kind of these basic sites (weak, medium, or strong ones) for performing the reaction is also discarded since the normalized values still indicate a different activity depending on the catalyst. A more complex scenario is suggested, in which a correct vicinity and interaction between acid and base sites (base/acid pairs) control the main activity. According to this hypothesis, the activity could be modulated using mixtures of catalysts.

All these conversions fit a first-order kinetic model (Figure 1b), meaning that the formation of a carbanion from the acetone molecule is the controlling step regardless of the mechanism followed (acid or basic catalysis), in good agreement with the previous literature.[12,24] This fit is also acceptable for $\beta$-zeolite, with a regression coefficient of $r^2$ = 0.97 (not significantly lower than the one obtained for MgAl, MgO, or $TiO_2$, with 0.984, 0.969, and 0.995, respectively). This conclusion is also relevant to propose a complex configuration, considering that different rate-limiting steps could imply an additional drawback, mainly the mechanical mixture configurations.

Conversion evolutions (Figure 2) indicate that all the materials deactivate, observing a decrease of the acetone converted with the TOS. In all cases, the temporal progress can be divided into two different phases: the first one with a clear decreasing trend (start-up phase) that could be fitted to an exponential evolution (first 3 h TOS, approximately) and the second one with a soft linear drop with almost uniform conversion (stable phase). This hypothesis is consistent with an almost stable activity once these mass-transfer limitations are not relevant, with a residual activity due to the external active sites. This double behavior can be depicted through a first-order deactivation kinetic model (eq 5)


https://doi.org/10.1021/acscatal.1c03095
ACS Catal. 2021, 11, 11650−11662

$$(x - x_\infty) = (x_0 - x_\infty)\cdot e^{(-k_d \cdot t)} \quad (5)$$

An alternative explanation of these two phases could be related to a fast and specific deactivation of strong sites, mainly by oligomerization, reaching a stable phase in which only medium-strength and weak sites are involved in the catalytic activity. This hypothesis could be true for basic materials in which there is a clear difference between weak and strong sites, but it could be discarded even in this case since the product distribution (discussed below) indicates a continuous production of C9 compounds (those that require strong active sites). In the case of these acid materials, all the acid sites are related to protons, having the same intrinsic "acidity" or strength. The differences in these materials are mainly due to confinement effects but not the strength and, with this, any different reactivity. Based on this discussion, the initial mass-transfer limitation influence is suggested as the main reason for the deactivation profiles observed.

Experimental data fit this model, obtaining a good fit (broken lines in Figure 2). The two parameters of this model, the residual or stable acetone conversion and the first-order deactivation rate constant ($x_\infty$ and $k_d$, respectively; values detailed in Table 2), are strongly affected by the temperature and the type of catalyst used, as observed in Figure 3. The temperature has a positive effect on the stable acetone conversion, obtaining higher values with acid materials than with basic ones. At temperatures lower than 350 °C, no significant differences between both types of materials were observed (close to 12% for basic materials and 22% for acid ones at 300 °C), with the remaining activity being more different as the temperature increases, reaching values of 43% for Al-MCM and 30% with $\beta$-zeolite at 400 °C. At this temperature, values lower than 25% were obtained with the basic materials. Concerning the $k_d$, three different behaviors are observed. Thus, the deactivation rate obtained for acid materials strongly decreases with the temperature with a similar evolution, whereas an increase is observed with the basic materials (MgO and MgAl), being more stressed for the most basic catalyst (MgAl). The intermediate behavior perceived with $TiO_2$, without observing a clear trend (the deactivation rate decreases from 200 to 300 °C, with an increase at higher temperatures), suggests that this material has an activity mainly conditioned by its redox properties and not only the basic ones. The interest of redox materials to enhance condensations has been previously demonstrated in the literature, observing promising results since the redox properties can help to stabilize oxygenated anions, enhancing the activity of the basic sites.[25,26]

**Table 2. Kinetic and Deactivation Parameters for All the Materials Tested as a Function of the Temperature**

| $\beta$-zeolite | 200 °C | 250 °C | 300 °C | 350 °C | 400 °C |
|---|---|---|---|---|---|
| $r_0$ ($h^{-1}$) | 4.5 | 5.7 | 6.1 | 6.4 | 6.5 |
| $x_\infty$ | 0.13 | 0.17 | 0.21 | 0.27 | 0.30 |
| $k_d$ | 2.01 | 1.58 | 1.05 | 0.91 | 0.46 |
| Al-MCM | 200 °C | 250 °C | 300 °C | 350 °C | 400 °C |
| $r_0$ ($h^{-1}$) | 34.1 | 36.5 | 42.1 | 44.0 | 50.1 |
| $x_\infty$ | 0.1 | 0.18 | 0.24 | 0.30 | 0.43 |
| $k_d$ | 2.21 | 1.37 | 1.14 | 0.65 | 0.59 |
| $TiO_2$ | 200 °C | 250 °C | 300 °C | 350 °C | 400 °C |
| $r_0$ ($h^{-1}$) | 34.9 | 43.5 | 54.4 | 67.5 | 75.8 |
| $x\infty$ | 0.05 | 0.06 | 0.10 | 0.17 | 0.26 |
| $k_d$ | 0.85 | 0.76 | 0.53 | 0.59 | 0.79 |
| MgAl | 200 °C | 250 °C | 300 °C | 350 °C | 400 °C |
| $r_0$ ($h^{-1}$) | 12.9 | 18.3 | 26.2 | 28.7 | 38.0 |
| $x_\infty$ | 0.05 | 0.07 | 0.10 | 0.11 | 0.18 |
| $k_d$ | 0.85 | 0.78 | 1.00 | 1.34 | 1.86 |
| MgO | 200 °C | 250 °C | 300 °C | 350 °C | 400 °C |
| $r_0$ ($h^{-1}$) | 67.6 | 26.6 | 41.5 | 51.7 | 67.6 |
| $x_\infty$ | 0.06 | 0.09 | 0.13 | 0.17 | 0.21 |
| $k_d$ | 0.37 | 0.45 | 0.72 | 0.74 | 1.03 |

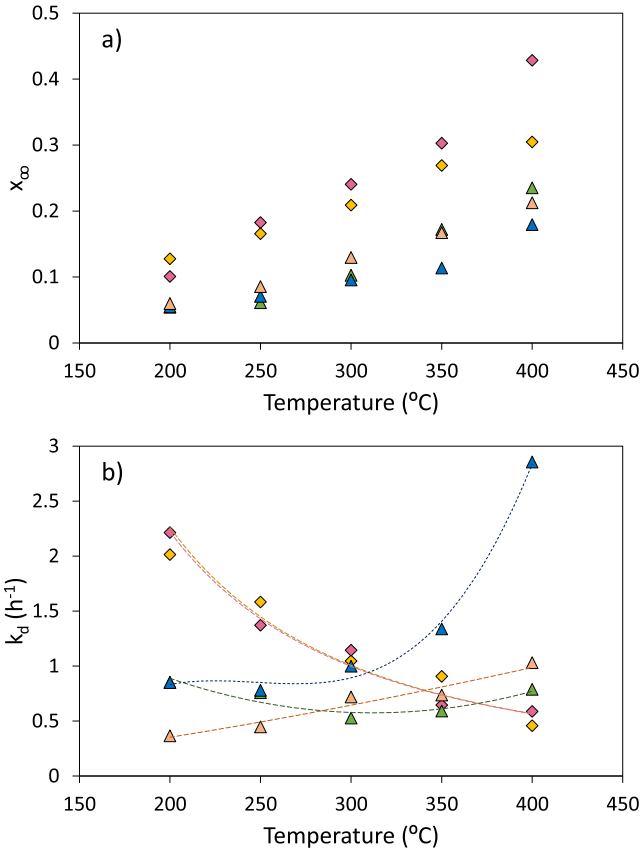


**Figure 3.** Evolution of (a) stable conversion and (b) first-order deactivation rate constant as a function of the temperature and the catalyst used for the acetone self-condensation. Symbols: (orange ◆) $\beta$-zeolite, (pink ◆) Al-MCM, (green ▲) $TiO_2$, (blue ▲) MgAl, and (peach ▲) MgO. Dashed lines in (b) are only included to guide the eye.

These results suggest the presence of two different deactivation processes. As for acid materials, the decreasing trend and its shape with the temperature indicate that the deactivation is related to secondary reactions, that is, because of the formation of intermediate species at low temperatures that lead to carbonaceous deposits if the reaction conditions are not severe enough to promote a subsequent step along the reaction mechanism. According to the reaction pathway, the reactivity of mesityl oxide and phorones in the presence of acid catalysts is analysed, concluding that mesityl oxide can produce not only C9 compounds but also alkenes and acetic acid by the $\beta$-scission side reaction. To a lower extent, this cracking can also be produced from linear phorones, obtaining similar types of compounds. Thus, temperature appears to be a key parameter to control the evolution of both pathways. The previous literature confirms by diffuse reflectance infrared Fourier transform spectroscopy the strong adsorption of both


https://doi.org/10.1021/acscatal.1c03095
ACS Catal. 2021, 11, 11650−11662

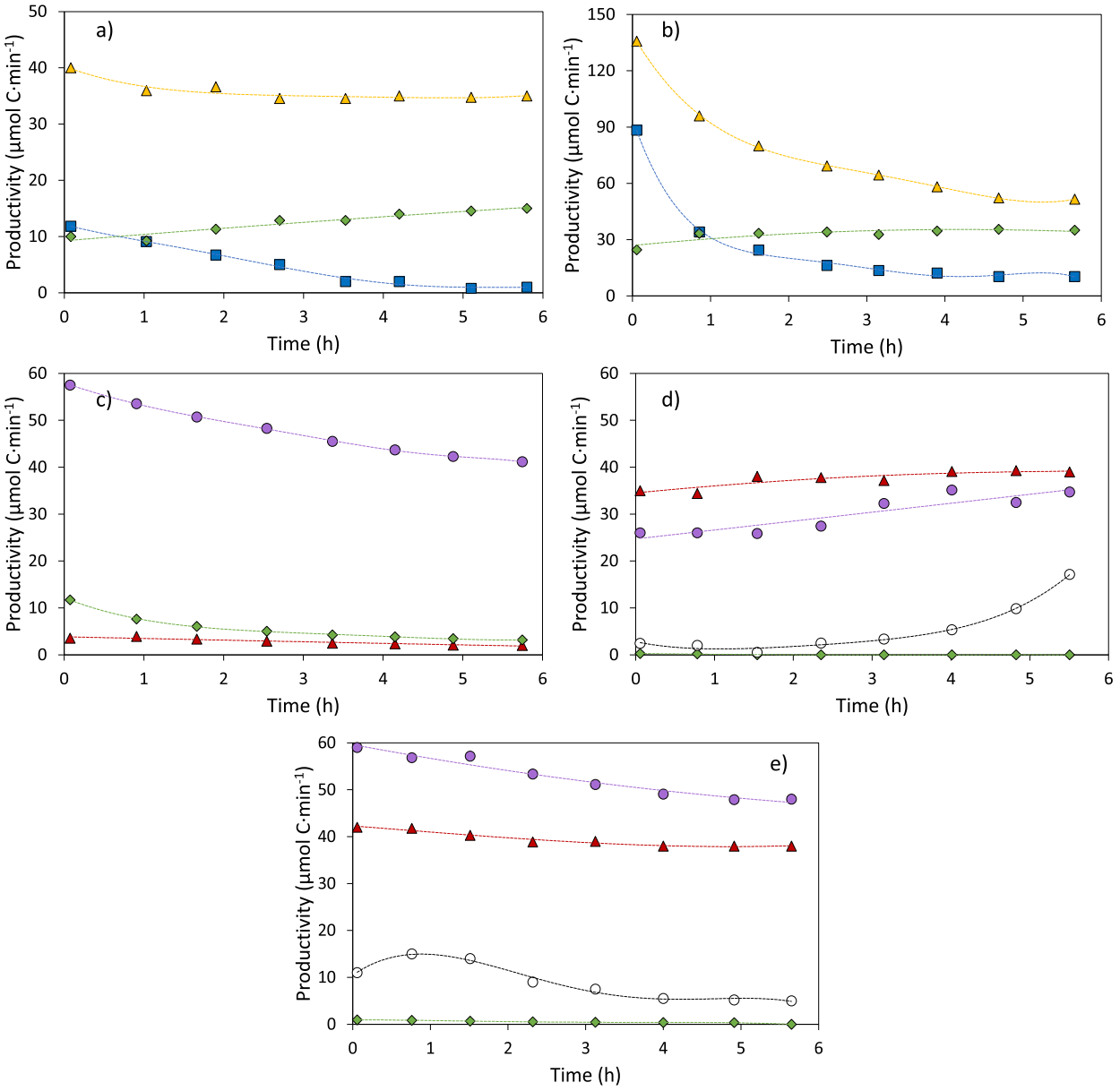


**Figure 4.** Time evolution of the main compounds obtained in the acetone self-condensation at 300 °C with (a) $\beta$-zeolite, (b) Al-MCM, (c) $TiO_2$, (d) MgAl, and (e) MgO. Symbols: (violet ●) mesityl oxide; (◯) phorones; (brown ▲) isophorones; (green ◆) mesitylene; (black ■) acetic acid; (orange ▲) isobutene.

compounds on an acid surface and the presence of oligomers derived from acetic acid, a consequence of the high interaction of the metal cations of the catalytic surface (Lewis sites) and the carboxylic functional group.[10,16,20]

This discussion agrees with the evolution of the gas-phase concentration of the different compounds involved in the reaction catalyzed by Al-MCM. Figure 4 shows these evolutions at 300 °C as an example; all the profiles are included in the Supporting Information (Figures S1−S5). Isobutene and acetic acid are the main compounds detected at initial times with Al-MCM, observing a fast decrease with time. These compounds are obtained in equimolar amounts by the $\beta$-scission; differences observed are justified by selective adsorption of acetic acid, blocking the active sites responsible for their formation (Lewis sites). On the contrary, mesitylene follows a constant profile, suggesting that its production depends on more stable active sites (protons).

Comparing these results with those obtained using $\beta$-zeolite, the relevance of the position of each site on the catalytic surface is also suggested. The molecular size of mesitylene is higher than the voids of this zeolite (8.7 and 6.7 Å, respectively).[10] The positive trend of its conversion reveals that its formation happens on the external acid sites, and these sites are not affected by the deactivation. According to this, the mesityl oxide cracking occurs on the active sites located at the internal surface of $\beta$-zeolite without affecting the main reaction pathways. With this material, the differences between isobutene and acetic acid profiles support the previous hypothesis about a deactivation mainly due to the acetic acid oligomerization.

A similar situation is obtained regardless of the temperature analyzed, with constant profiles of mesitylene. However, the relevance of the side reaction increases with the temperature, obtaining a lower production of the target compound and a


https://doi.org/10.1021/acscatal.1c03095
ACS Catal. 2021, 11, 11650−11662

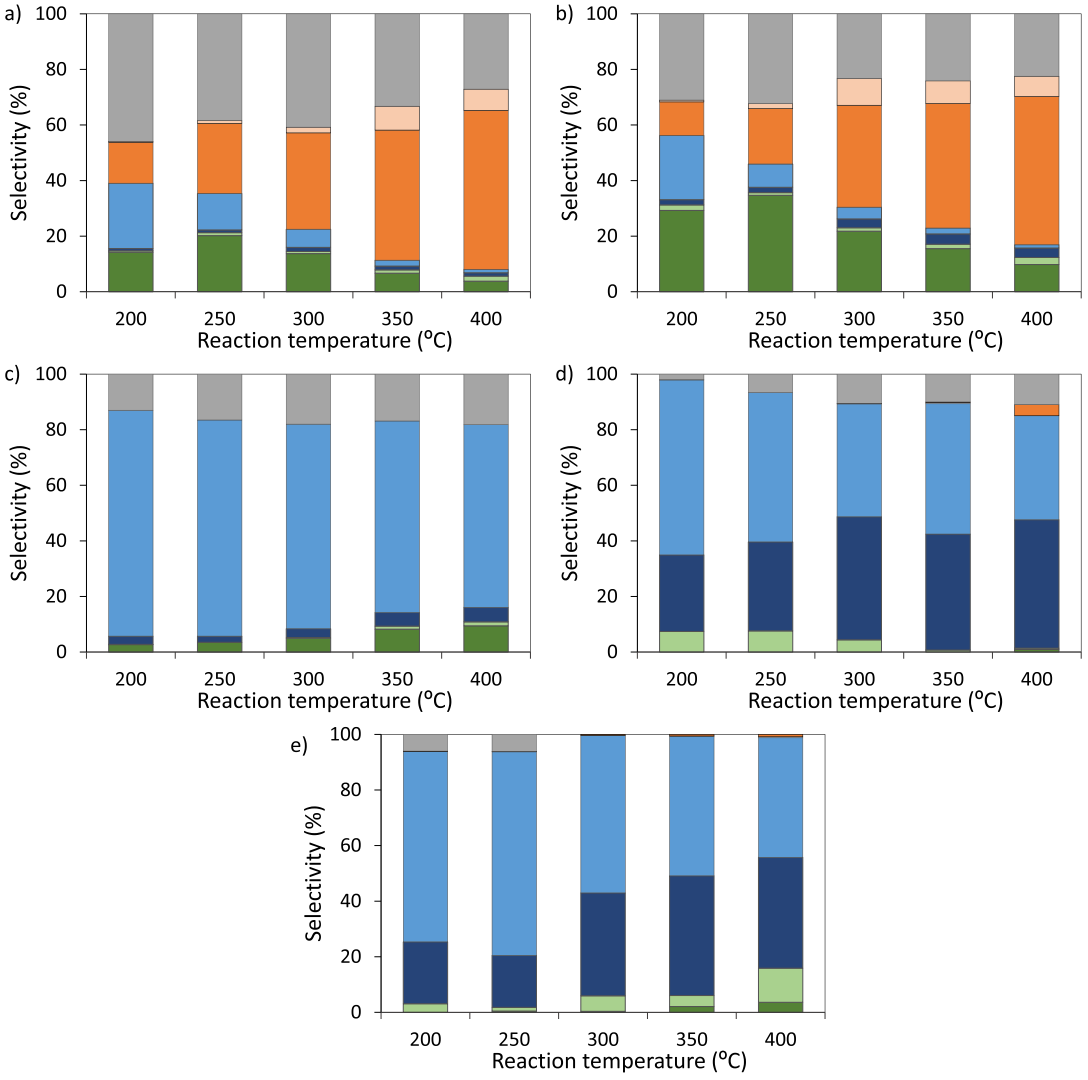


**Figure 5.** Analysis of the product distribution once the stable phase is reached (~3 h of TOS) as a function of the temperature. The results are expressed in carbon selectivity terms. Values correspond to data obtained with (a) $\beta$-zeolite, (b) Al-MCM, (c) $TiO_2$, (d) MgAl, and (e) MgO. Legend: mesitylene (dark green), mesitylene isomers (light green), phorones and isophorones (dark blue), mesityl oxide (light blue), isobutene (dark orange), acetic acid (light orange), and COx & coke (gray).

higher production of acids and light alkenes. To sum up, $\beta$-scission has more influence as a lateral route (decreasing the selectivity) than as a deactivation cause. The decrease in the deactivation rate with the temperature is justified since adsorption is an exothermic process, and high temperatures promote the desorption of these alkenes, preventing the blockage of the active sites. The remaining deactivation is due to acetic acid since temperature enhances the polymerization. Accordingly, the stoichiometric production of these two side products is never detected in the gas phase. To conclude, the stability obtained at high temperatures is not related to an increase in the main route.

On the other hand, base materials deactivate because of the stable adsorption (with or without oligomerization) of different compounds. Considering the positive effect of the temperature, the products adsorbed could be those that require more harsh conditions for their production (final products, isophorones and/or mesitylene). However, if the deactivation is due to oligomerizations, intermediate products such as phorones could be also involved. In both cases, strong basicity promotes these effects,[12] justifying the relevant deactivation observed with MgAl, a material with a concentration of these sites more than 3 and 7 times higher than the corresponding ones of MgO and $TiO_2$, respectively. Comparing the evolution of main compounds shown in Figure 4, MgAl highlights as the catalyst that promotes the highest amount of isophorones, reaching a flat evolution in less than 2 h. The absence of mesitylene, despite the presence of acid sites, indicates that this isophorone corresponds to the $\beta$-isomer (the one that does not isomerize into mesitylene). Considering that both isophorones are in equilibrium, the strong adsorption of the $\alpha$-isomer as well as the corresponding one of linear phorones is assumed to be the main deactivation cause in this case. The $\alpha$-isomer is observed in the gas phase with $TiO_2$ and MgO, with the corresponding decrease in the deactivation rate (mainly in the case of $TiO_2$ or mesitylene). All this discussion is supported by the concentration profiles and selectivity distribution detailed in the Supporting Information (Figures S1−S5, Table S2).

The presence of two different deactivation precursors is in good agreement with the TPO profiles of the spent catalysts, shown in Figure S6. The decomposition of the main carbonaceous deposits produced on the base materials


https://doi.org/10.1021/acscatal.1c03095
ACS Catal. 2021, 11, 11650−11662

corresponds to temperatures from 250 to 450 °C, whereas the main peak observed with acid materials is significantly more stable, with decomposition temperatures around 550 °C. The previous literature indicates that the first range corresponds to dimers and trimers adsorbed on the catalytic surface producing disordered and unstable solids,[17] whereas the oligomerization of small molecules produces well-ordered deposits, requiring higher temperatures to produce their decomposition. These deposits are much more relevant in the case of β-zeolite, a microporous material in which confinement effects play a key role in stabilizing coke precursors.

Figure 5 shows the selectivities once the stable phase has been reached (~3 h of TOS). Mesityl oxide is the main product obtained with $TiO_2$, with 81.3% selectivity at 200 °C. At this temperature, less than 6% corresponds to linear and aromatic compounds, with almost 50% of mesitylene and isophorones. The mesityl oxide selectivity slowly decreases as the temperature increases, reaching a minimum of 65.7% at 400 °C. This decrease does not correspond to a significant amount of unknown peaks (COx & coke fraction), compounds that are almost stable at 18%. Thus, there is an increase in the production of the desired compounds, with a maximum of 9.4% of mesitylene and 5.2% of phorones and isophorones. Only at the harshest temperatures, traces of mesitylene isomers (other alkylbenzenes) are detected, being lower than 2% in any case.

In the case of MgAl, the highest concentration of base sites justifies the higher relevance of C9 (phorones and isophorones) regardless of the temperature tested. At 200 °C, mesityl oxide corresponds to 65%, with more than 27.5% of phorones and isophorones. This fraction increases with the temperature, at the expense of C6, reaching the maximum at 400 °C, with a total selectivity of 46.2%. Mesitylene is not detected at any temperature, observing only small amounts of other trialkylbenzenes at the lowest temperatures (7% at 200 °C). These data confirm the role of strong basicity promoting the second condensation.

MgO produces a similar evolution, but the low strong basicity of this material restricts the results. Thus, the initial amount of mesityl oxide is slightly higher than that with MgAl (69% at 200 °C), and the second condensation to produce C9 is less favorable than that with MgAl, reaching a minimum C6's selectivity of 43%, with a corresponding 40% of oxygenated C9s. The most relevant difference is linked to the carbon balance, reaching almost 100% at temperatures higher than 250 °C, suggesting a higher control on the reaction products. Furthermore, the selectivity toward trialkylbenzenes increases with the temperature, with more than 12% at 400 °C. At this temperature, small traces of mesitylene are also observed (4%).

The different behavior of the three basic materials is justified by the particular contribution of each phoronic compound to the total C9 group. These data are included in the Supporting Information, in Table S2. MgAl only produces β-isophorone, observing only traces of the α-isophorone at the lowest temperatures (less than 3% of relative selectivity). At this temperature, the acidity is not sufficiently active to produce the dehydration required to obtain mesitylene. On the other hand, relevant relative selectivities of the α-isophorone are obtained with $TiO_2$ (100% at 200 and 250 °C, decreasing to 41% at 400 °C) and in less amount with MgO (relative selectivities from 4 to 10%). This compound is identified as the main intermediate in mesitylene production.

As for the acid materials, similar distributions are obtained with β-zeolite and Al-MCM catalysts, in the first case with a higher carbon unbalance, explained by more relevant molecule confinement inside the channels of the zeolite. These unidentified permanent gases or solid deposits are produced in a significantly higher amount with acid materials, being close to 50% with β-zeolite and higher than 30% with Al-MCM. In both cases, mesitylene is obtained in large amounts, reaching maximum values of 35% and 20%, with Al-MCM and β-zeolite materials, respectively, with both at 250 °C. These maximums at an intermediate temperature suggest the competition between adsorption (promoted at low temperatures) and side reactions, mainly the β-scission, with both mechanisms at the expense of the main reaction route. In fact, the β-scission is relevant at all the temperatures tested, showing a clear increasing trend, reaching maximums of 60 and 61%, with Al-MCM and β-zeolite at 400 °C, respectively. Considering the decreasing selectivity of C6 and the lack of correspondence with an increase in the C9s, a competitive mechanism between β-scission and the second condensation is suggested in such a way that most of the mesityl oxide produced with these materials is transformed into undesired compounds. The high concentration of acid sites justifies the almost total absence of phorones and isophorones, promoting the dehydration of both compounds into the target compound and, in less amount, other isomers.

A global analysis of activity and stability results reveals opposite advantages and disadvantages of working with acid and basic materials. β-Zeolite is discarded because of its relevant confinement limitations, whereas Al-MCM is a promising catalyst to the selective production of C9, working at 250 °C, the temperature at which the drawback because of the β-scission is limited. In any case, this side reaction implies more than 20%, suggesting the need for a first catalytic bed that adjusts the stream properties, preventing the formation of β-scission precursors on the acid surface. Considering the high production of C9 (mesitylene precursors) produced with basic materials and the absence of side reactions with these materials, the combination of both catalysts could imply an improvement of the mesitylene production and the reaction stability.

**Operation with Mixtures of Acid and Basic Catalysts.** Considering the previous premises, different catalytic mixtures have been tested, with the common point of including Al-MCM as an acid material (owing to its better performance than β-zeolite). Mechanical mixtures and a double-bed configuration are compared to determine the vicinity requirements. Since the basic materials tested also have acid properties, the chemical mixture to obtain a molecular vicinity is discarded, considering the physical mixture as the most promising alternative, promoting the scavenging movement required to tune the reaction to the main route, reducing the deactivation. In the double bed, the base catalyst is located in the first place, expecting to prevent the side reaction on the acid catalyst once the C9-enriched stream interacts with the second bed. The low temperature of these analyses (250 °C) is chosen considering the minimum deactivation observed with basic materials and assuming that the deactivation observed with Al-MCM (working alone) is mainly conditioned by the β-scission-derived compounds, intermediates that should be minimized with these strategies. As for the base materials, the inconclusive analysis of the individual studies prevents determining an optimum one. MgAl maximizes the C9


https://doi.org/10.1021/acscatal.1c03095
ACS Catal. 2021, 11, 11650−11662

production, whereas the C9 distribution and the carbon balance appear to be more favorable with MgO. However, a second acid material could promote the isophorone isomerization, promoting the mesitylene formation from MgAl. On the other hand, if the phorone production is relevant to increase the mesitylene yield, $TiO_2$ could be a good candidate, yielding a mixture enriched in mesityl oxide that could be transformed in phorones and dehydrated over the Al-MCM sites, without the intermediate step of isophorones, compounds that require strong basicity to be obtained.

Figure 6 shows the temporal profile of acetone conversion obtained for the six different configurations tested: three

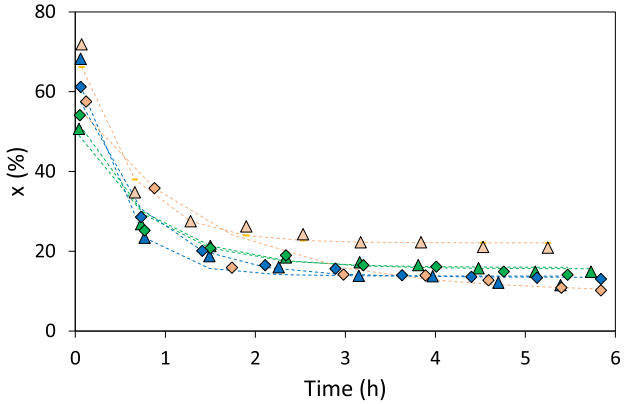


**Figure 6.** Evolution of acetone conversion with TOS at 250 °C as a function of the reaction system. Triangles represent double beds, whereas mechanical mixtures are identified as diamonds. All include Al-MCM as the acid catalyst, with $TiO_2$ (green), MgAl (blue), and MgO (orange) as basic catalysts. Dashed lines correspond to first-order deactivation kinetic model.

double-bed and three mechanical mixtures, combining in both cases a base material ($TiO_2$, MgAl, MgO) with Al-MCM. The fitted values are included in Figure 6 as broken lines. In this figure, original data with each catalyst have been included for comparison reasons. The deactivation model previously discussed has been applied to these data, obtaining the deactivation parameters analyzed in Figure 7.

As first insight, the conversion should increase with the catalytic loading following an exponential trend. According to this, the results obtained with the mechanical mixtures can be directly compared with those of the isolated catalysts, but in the case of the double-bed configuration, the results should be analyzed considering that there is a double amount of the catalyst compared to that with the original configuration (200 mg of the basic material + 200 mg of the acid one). As the objective is related to the mesitylene selectivity, the lack of proportionality in terms of conversion between single and double beds indicates that the reaction mechanism is modified by the co-presence of two materials. In other words, there is an effect because of the mixture of both catalysts (if each bed works as an isolated one, conversions should be additive). The lowest interaction is observed when using MgO as the base phase, with a slight decrease of 4.6% between the experimental value (71.9%) and the anticipated sum of both initial ones (75.4%). On the contrary, the initial conversion obtained with $TiO_2$ + Al-MCM (50.7%) is 31.8% lower than the theoretical one, with the configuration suggesting the most obvious interaction between both materials.

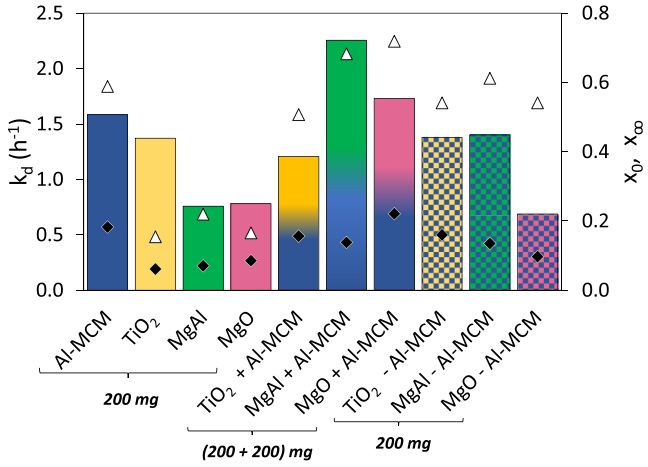


**Figure 7.** Analysis of conversion results as a function of the catalytic system used, considering the first-order deactivation rate constant ($k_d$), the initial conversion ($x_0$), and the stable conversion ($x_\infty$). Data correspond to double beds (materials isolated by +) and mechanical mixtures (−).

These results suggest that equilibrium between aldolization and retroaldolization reported in the literature[27] is more relevant when using the Al-MCM acid sites in such a way that a stream enriched in mesityl oxide coming into the acid bed (see the original distribution of $TiO_2$) reduces the advance to the following steps, producing the reverse reaction, obtaining acetone, and limiting the conversion. This hypothesis has been confirmed by introducing only mesityl oxide on the Al-MCM bed; the selectivity distribution is summarized in the Supporting Information (Figure S7), obtaining 14% of acetone selectivity and high relevance of back-cracking with a total selectivity toward isobutene and other alkenes higher than 44%.

As for the deactivation rate constants ($k_d$), the highest value is obtained with MgAl + Al-MCM (2.25 $h^{-1}$), whereas the smallest one corresponds to $TiO_2$ + Al-MCM (1.2 $h^{-1}$). This last configuration is the only one that produces a decrease in the deactivation rate, being suggested as the optimum one from this point of view. To support this statement, the TPO analyses of each catalyst of the double-bed configuration (broken lines) are analyzed in Figure 8 with the corresponding ones of the isolated materials. The solids deposited on $TiO_2$ when this material takes part in a double-bed configuration produces almost half of the $CO_2$ produced when this material works alone. There is also a decrease for solids deposited on Al-MCM, more relevant in those related to acetic acid oligomers (the highest temperature).

The worst situation obtained using MgAl suggests that a significant fraction of solid deposits is obtained from those C9 produced with this material, with the acid sites of Al-MCM being then the catalytic sites to promote their oligomerization. This result is also consistent with the TPO results, observing a higher signal of $CO_2$ after the TPO of Al-MCM when this material is part of a double-bed configuration. Moreover, the combustion temperature of the main peak (412 °C) decreases to values close to those corresponding to trimer adsorption, suggesting a change in the type of deactivation on the acid material, with a lower contribution of the $\beta$-scission and a higher relevance of heavy compound adsorption. The decrease in the solids left behind on MgAl is lower than the one observed with $TiO_2$, suggesting a lower interaction between


https://doi.org/10.1021/acscatal.1c03095
ACS Catal. 2021, 11, 11650−11662

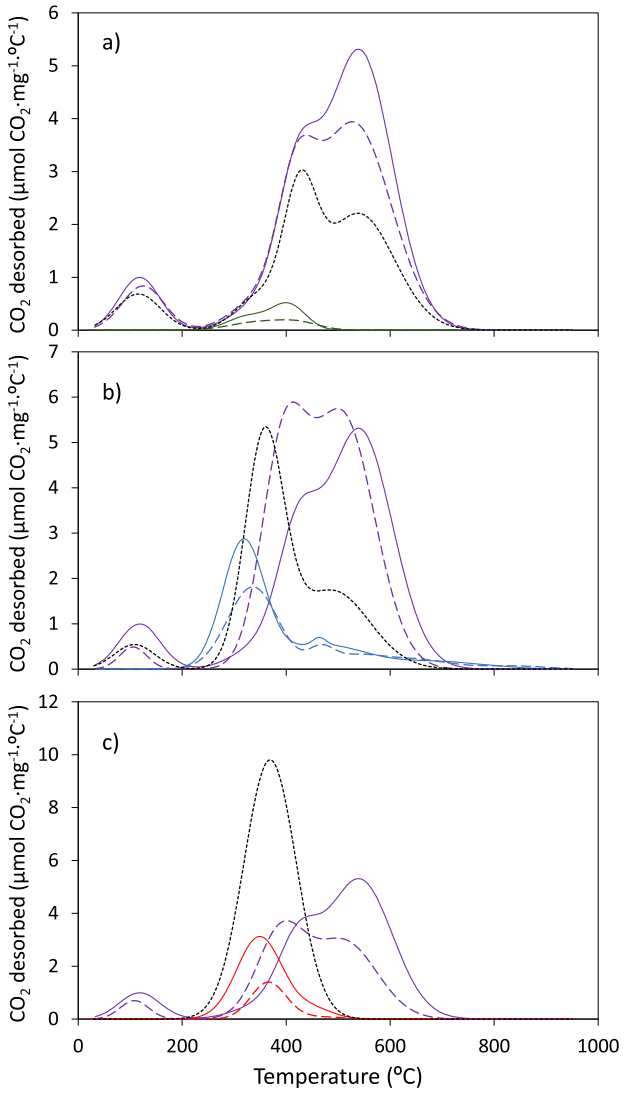


**Figure 8.** TPO analyses of (a) $TiO_2$ + Al-MCM, (b) MgAl + Al-MCM, and (c) MgO + Al-MCM. Legend: $TiO_2$ (green), MgAl (blue), MgO (red), and Al-MCM (violet). Dashed lines correspond to the catalyst taking part in a double bed, continuous lines indicate the results obtained with isolated materials, and black dotted lines correspond to the mechanical mixtures.

both beds and a MgAl behavior very similar, irrespective of being alone or in multiple configurations. The same effect is observed with MgO but to a significant lower extent.

As discussed in the first part of the paper, the deactivation model proposed considers a residual acetone conversion. The differences in these values, with conversions for all the double beds higher than those for the base materials, support the previous idea that the relevant deactivation mainly blocks the strong basic sites, with the catalyst keeping a stable conversion if it has sufficient acid sites. The stable conversion obtained with MgO + Al-MCM (22.4%) is higher than the original one obtained with Al-MCM (17.8%), whereas similar values are obtained with the two remaining systems, in agreement with the prevalence of an activity related to acid conversion.

Concerning the mechanical mixtures, the same amount of the catalyst (200 mg) is used in all the cases. A clear improvement in the expected conversion is observed in all the cases, being more evident in the MgAl−Al-MCM system (61.1, 51.5% higher than the theoretical value, 40.4%). Values reached with $TiO_2$−Al-MCM and MgO−Al-MCM (around 54% in both cases) are significantly higher than those expected considering a 50% contribution of each raw catalyst. These results confirm the relevance of reaction equilibria in such a way that the vicinity between different types of sites allows the advance in the reaction, altering the initial equilibria between condensation and retroaldolization of hydration and dehydration steps. In good agreement with this hypothesis, the highest conversion is reached with the system involving the strongest basic sites (MgAl−Al-MCM) since they produce a higher amount of C9 that is not easily decomposed, whereas for those in which mesityl oxide prevails over the phorones, the co-presence of acid sites catalyzes the retroaldolization, observing a slightly lower acetone conversion.

The system MgO−Al-MCM demonstrates a slower deactivation, 0.69 $h^{-1}$, whereas very similar rates are obtained with the other two materials (1.4 $h^{-1}$), a bit higher than the expected value. On the contrary, MgO−Al-MCM deactivates to a stable conversion (9.7%) significantly lower than the other mechanical mixtures, with values of 16 and 13.5%, for $TiO_2$−Al-MCM and MgAl−Al-MCM, respectively. These values are 12% higher than the expected values, reinforcing the effect of this configuration. TPO profiles support these results, observing an increase in the $CO_2$ signal of the MgO−Al-MCM mechanical mixture, focused on the temperatures related to the strong adsorption of C9, whereas the other two cases demonstrate a total amount of solid deposits lower than the sum of both compounds (isolated and in a double-bed configuration), with a relevant signal related to well-ordered carbonaceous deposits.

The most relevant improvements are, however, obtained in terms of selectivity. The product distributions once reaching the stationary phase are shown in Figure 9. The temporal

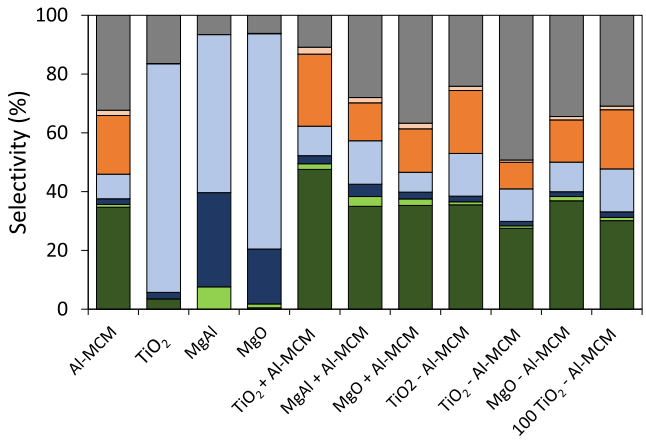


**Figure 9.** Analysis of the product distribution in carbon selectivity terms obtained at 250 °C. Legend: mesitylene (dark green), mesitylene isomers (light green), phorones and isophorones (dark blue), mesityl oxide (light blue), isobutene (dark orange), other alkenes (light orange), and COx & coke (gray).

evolutions of main compounds are included in the Supporting Information (Figures S8−S10). The presence of the $\beta$-scission is observed in all the cases, being more relevant using $TiO_2$ (in both configurations). This fact agrees with the higher mesitylene selectivity observed with this material. Comparing the results obtained with the double beds with those of mechanical mixtures, the prevalence of the second condensa-


https://doi.org/10.1021/acscatal.1c03095
ACS Catal. 2021, 11, 11650−11662

tion (strong basicity) over the side reaction (strong acidity) is observed, with lower selectivities to alkenes in the mechanical mixtures, when those active sites are very close (from 14.7 to 9.7% in the case of using MgAl). The lack of correspondence of this hypothesis with a higher amount of mesitylene suggests that most of the phorones and isophorones adsorbed on the acid sites promote coke formation instead of the dehydration to mesitylene. This is corroborated by the higher proportion of $\beta$-isophorone and the 2,6-dimethyl-2,5-heptadien-4-one phorones, the isomers with the ketone group in the intermediate position (these ratios are detailed in Table S2). Consequently, the percentage of carbon unbalance increases significantly, mainly in those systems including strong basic materials, that is, MgAl.

In terms of mesitylene selectivity, a relevant improvement is observed with the double bed involving $TiO_2$, obtaining a final mixture enriched in the target compound (47.6 vs 34.7% of the initial Al-MCM). Moreover, this system significantly reduces the coke produced when using only Al-MCM, reaching a final mixture in which light alkenes are the secondary products (26.5%). This fact is a relevant improvement from the point of view of stream purification, being also considered as a positive consequence of working with this configuration.

This result could be unexpected since isolated results obtained with $TiO_2$ revealed that this material provides the lowest amount of phorones and isophorones, the natural precursors of mesitylene. On the contrary, almost 80% of acetone converted is transformed into mesityl oxide. A particular experiment has been carried out with the Al-MCM catalyst to analyze this effect, feeding a mixture of mesityl oxide and acetone, with both reactants being 10% of the total flow. The selectivity distribution, detailed in the Supporting Information (Figure S10), shows a high production of mesitylene, obtaining almost total conversion of mesityl oxide (a selectivity of 4%), and a stable selectivity to mesitylene and other isomers higher than 35%. This result suggests that the second condensation (from mesityl oxide to phorones) is a rapid reaction; that is, the $\alpha$-proton abstraction of mesityl oxide is easier than the corresponding one from acetone. The high unsaturation character of mesityl oxide in comparison to acetone as well as the possibility to isomerize into isomesityl oxide promotes the adsorption of this compound on the catalytic surface (a fact experimentally corroborated in a previous work),[17] increasing the stability of the intermediate required to produce the condensation, by both the acid and basic mechanisms. Thus, the second condensation is easier than the first one. According to this premise, the high production of phorones and isophorones on the catalytic bed is not as important as the corresponding one of mesityl oxide, with the first ones being more related to the coke formation than to the mesitylene one.

In global terms, despite the slight increase in the deactivation rate observed with this configuration, the double-bed $TiO_2$ + Al-MCM is proposed as the optimum system, obtaining a clear improvement in the mesitylene selectivity once the stable phase is reached. The synergetic effect between these two materials is confirmed since the stable conversion is almost the same as that working with only the acid phase, but the selectivities have a different distribution and the amount of coke produced is also limited. All the systems were kept for 6 h, obtaining a total mesitylene production of 0.22 g/g acetone converted, a value more than 57% higher than the corresponding one when only using the Al-MCM material.

## CONCLUSIONS

The study of the acetone self-condensation with basic and acid catalysts allows to conclude that acid materials are required to promote the last steps of the process (isomerization, dehydration, and cyclization). However, the absence of basicity promotes the $\beta$-scission reaction, mainly at a high temperature. The acetic acid produced consumes mesityl oxide, reducing the productivity, and it is involved in the Lewis acidity blockage by oligomerization, without a relevant effect on the catalytic deactivation since this reaction depends on Brønsted sites.

Basic catalysts do not produce a significant amount of mesitylene but a high selectivity to its promoters (phorones and isophorones). With these materials, high temperatures condition the stability by phorones and isophorone stable adsorption.

These partial conclusions allow proposing an optimum configuration based on the synergetic effect of a double bed of $TiO_2$ and Al-MCM as the basic and acidic components, respectively. The first catalyst promotes the condensations, producing an optimum mixture of mesityl oxide, acetone, and phorones that are selectively transformed into mesitylene on the acid moiety. This configuration produces a stable system in which the deactivation is minimized, with an increase in the mesitylene productivity higher than 57% compared with the parent Al-MCM material.

## ASSOCIATED CONTENT

### Supporting Information

The Supporting Information is available free of charge at https://pubs.acs.org/doi/10.1021/acscatal.1c03095.

Detailed profiles of the reaction product productivity with reaction time for all the catalysts and catalyst combinations tested in this work, TPO profiles of the studied catalysts after reaction, numerical analysis of internal and external mass-transfer effects, and detailed isomer distribution for phorones and isophorones (PDF)

## AUTHOR INFORMATION


### Corresponding Author

**Salvador Ordóñez** − *Catalysis, Reactors & Control Research Group (CRC), Department of Chemical and Environmental Engineering, University of Oviedo, Oviedo 33006, Spain;* orcid.org/0000-0002-6529-7066; Email: sordonez@uniovi.es

### Authors

**Laura Faba** − *Catalysis, Reactors & Control Research Group (CRC), Department of Chemical and Environmental Engineering, University of Oviedo, Oviedo 33006, Spain*

**Juan Gancedo** − *Catalysis, Reactors & Control Research Group (CRC), Department of Chemical and Environmental Engineering, University of Oviedo, Oviedo 33006, Spain*

**Jorge Quesada** − *Catalysis, Reactors & Control Research Group (CRC), Department of Chemical and Environmental Engineering, University of Oviedo, Oviedo 33006, Spain*

**Eva Diaz** − *Catalysis, Reactors & Control Research Group (CRC), Department of Chemical and Environmental Engineering, University of Oviedo, Oviedo 33006, Spain*

Complete contact information is available at:
https://pubs.acs.org/10.1021/acscatal.1c03095

### Notes

The authors declare no competing financial interest.

## ■ ACKNOWLEDGMENTS

We acknowledge the financial support from the Spanish Ministry of Science and Innovation (CTQ2017-89443-C3-2-R and PDC2021-120835-C21) and the regional Government of the Principality of Asturias (IDI/2018/000116).

## ■ REFERENCES

(1) Ivakhnov, A. D.; Skrebets, T. E.; Bogdanov, M. V. Dehydrocondensation of acetone under supercritical conditions. *Russ. J. Phys. Chem. B* **2019**, *13*, 1125−1127.
(2) Berris, B. C. Phenolic antioxidant and process. U.S. Patent 5,292,969 A, 1994, Current assignee: Albemarle Corp. US (Mar 8).
(3) Dodge, H. M.; Kita, M. R.; Chen, C.-H.; Miller, A. J. M. Identifying and evading olein isomerization catalyst deactivation pathways resulting from ion-tunable hemilability. *ACS Catal.* **2020**, *10*, 13019−13030.
(4) Biradha, K.; Fujita, M. A "three-in-one" crystal of coordination networks. *Chem. Commun.* **2002**, *17*, 1866−1867.
(5) Trilla, M.; Pleixats, R.; Parella, T.; Blanc, C.; Dieudonné, P.; Guari, Y.; Man, M. W. C. Ionic liquid crystals based on mesitylene-containing bis- and trisimidazolium salts. *Langmuir* **2008**, *24*, 259−265.
(6) Zhao, S.; Wang, W. D.; Wang, L.; Schwieger, W.; Wang, W.; Huang, J. Tuning hierarchical ZSM-5 zeolite for both gas- and liquid-phase biorefining. *ACS Catal.* **2020**, *10*, 1185−1194.
(7) Earhart, H. W.; Sugerman, G. Alkylation and isomerization process. U.S. Patent 3,542,890 A, 1970, Current assignee: Koch Industries Inc.
(8) Li, H.; Riisager, A.; Saravanamurugan, S.; Pandey, A.; Sangwan, R. S.; Yang, S.; Luque, R. Carbon-increasing catalytic strategies for upgrading biomass into energy-intensive fuels and chemicals. *ACS Catal.* **2018**, *8*, 148−187.
(9) Lanzafame, P.; Perathoner, S.; Centi, G.; Gross, S.; Hensen, E. J. M. Gran challenges for catalysis in the Science and Technology Roadmap on Catalysis for Europe: moving ahead for a sustainable future. *Catal. Sci. Technol.* **2017**, *7*, 5182−5194.
(10) Quesada, J.; Faba, L.; Díaz, E.; Ordóñez, S. Effect of catalyst morphology and hydrogen co-feeding on the acid-catalysed transformation of acetone into mesitylene. *Catal. Sci. Technol.* **2020**, *10*, 1356−1367.
(11) Li, G.; Ngo, D. T.; Yan, Y.; Tan, Q.; Wang, B.; Resasco, D. E. Factors determining selectivity of acid- and base-catalyzed self- and cross-condensation of acetone and cyclopentanone. *ACS Catal.* **2020**, *10*, 12790−12800.
(12) Faba, L.; Díaz, E.; Ordóñez, S. Gas phase acetone self-condensation over unsupported and supported Mg-Zr mixed-oxides catalysts. *Appl. Catal., B* **2013**, *142−143*, 387−395.
(13) Herrmann, S.; Iglesia, E. Selective conversion of acetone to isobutene and acetic acid on aluminosilicates: kinetic coupling between acid-catalyzed and radical-mediated pathways. *J. Catal.* **2018**, *360*, 66−80.
(14) Ordóñez, S.; Díaz, E.; León, M.; Faba, L. Hydrotalcite-derived mixed oxides as catalysts for different C-C bond formation reactions from bioorganic materials. *Catal. Today* **2011**, *167*, 71−76.
(15) Zamora, M.; López, T.; Gómez, R.; Asomoza, M.; Melendrez, R. Oligomerization of acetone over titania-doped catalysts (Li, Na, K and Cs): effect of the alkaline metal in activity and selectivity. *Catal. Today* **2005**, *107−108*, 289−293.
(16) Li, H.; Sun, J.; Wang, Y. Surface acetone reactions on ZnxZryOz: A DRIFT-MS study. *Appl. Catal., A* **2019**, *573*, 22−31.
(17) Quesada, J.; Faba, L.; Díaz, E.; Bennici, S.; Auroux, A.; Ordóñez, S. Role of Surface intermediates in the deactivation of MgZr mixed oxides in acetone self-condensation: a combined DRIFT and ex situ characterization approach. *J. Catal.* **2015**, *329*, 1−9.
(18) Quesada, J.; Faba, L.; Díaz, E.; Ordóñez, S. Effect of metal modification of titania and hydrogen co-feeding on the reaction pathways and catalytic stability in the acetone aldol condensation. *J. Catal.* **2019**, *377*, 133−144.
(19) Lin, F.; Wang, H.; Zhao, Y.; Fu, J.; Mei, D.; Jaegers, N. R.; Gao, F.; Wang, Y. Elucidation of active sites in aldol condensation of acetone over single-facet dominant anatase $TiO_2$ (101) and (001) catalysts. *JACS Au* **2021**, *1*, 41−52.
(20) Herrmann, S.; Iglesia, E. Elementary steps in acetone condensation reactions catalysed by aluminosilicates with diverse void structures. *J. Catal.* **2017**, *346*, 134−153.
(21) León, M.; Faba, L.; Díaz, E.; Bennici, S.; Vega, A.; Ordóñez, S.; Auroux, A. Consequences of MgO activation procedures on its catalytic performance for acetone self-condensation. *Appl. Catal., B* **2014**, *147*, 796−804.
(22) Scanlon, J. T.; Willis, D. E. Calculation of flame ionization detector relative response factors using the effective number concept. *J. Chromatogr. Sci.* **1985**, *23*, 333−340.
(23) Gounder, R.; Iglesia, E. The catalytic diversity of zeolites: confinement and solvation effects within voids of molecular dimensions. *Chem. Commun.* **2013**, *49*, 3491−3509.
(24) Wang, S.; Goulas, K.; Iglesia, E. Condensation and esterification reactions of alkanals, alkanones, and alkanols on $TiO_2$: elementary steps, site requirements, and synergistic effects of bifunctional strategies. *J. Catal.* **2016**, *340*, 302−320.
(25) Quesada, J.; Arreola-Sánchez, R.; Faba, L.; Díaz, E.; Rentería-Tapia, V. M.; Ordóñez, S. Effect of Au nanoparticles on the activity of $TiO_2$ for ethanol upgrading reactions. *Appl. Catal., A* **2018**, *551*, 23−33.
(26) Young, Z. D.; Hanspal, S.; Davis, R. J. Aldol condensation of acetaldehyde over titania, hydroxyapatite, and magnesia. *ACS Catal.* **2016**, *6*, 3193−3202.
(27) Noda Pérez, C.; Pérez, C. A.; Henriques, C. A.; Monteiro, J. L. F. Hydrotalcites as precursors for Mg-Al mixed oxides used as catalysts on the aldol condensation of citral with acetone. *Appl. Catal., A* **2004**, *272*, 229−240.